2024 IEEE International Conference on Robotics and Automation (ICRA 2024)
May 13-17, 2024. Yokohama, Japan

System Identification of Space Manipulator Systems and its Implications on Robust Control Performance*

Georgios Rekleitis[1], Evangelos Papadopoulos[1]

Abstract— **Space manipulator system (SMS) maneuvers can excite flexible appendages, while fuel sloshing effects impact its dynamics and performance. To predict this behavior and control such systems, sloshing and flexible appendages are modeled. A novel system identification scheme is developed, which identifies all parameters required for the reconstruction of system dynamics despite unmeasurable sloshing and modal states. This is achieved by two identification experiments. In Exp.1 all unmeasurable states are eliminated, while in Exp.2 the unmeasurable sloshing states are eliminated, and a novel estimator is used for the unmeasurable modal states. The significance of accurate SYSID in controller design and performance is demonstrated by simulating a 3D SMS controlled by model-based and robust controllers. In both cases, using the identified parameters results in significant robust control performance enhancement.**

I. INTRODUCTION

Accurate Space Manipulator System (SMS) maneuvering, tracking, and reduced control effort, require good knowledge of system properties. These may not be available always, due to inaccurate modelling, fuel sloshing or flexible appendage effects, [1], [2], [6], [8], [15]. Fuel consumption changes spacecraft (S/C) parameters significantly, while flexible appendage properties vary with temperature, both introducing uncertainties. Methods have been proposed to mitigate uncertainty (e.g., [3]) but cannot eliminate it. Accurate sloshing and appendage models coupled with S/C dynamics and accurate parameters are needed for control; their lack results in poor performance or instabilities [4], [8].

Fluid behavior as a function of acceleration is complex, making accurate fluid motion modeling in zero-gravity very difficult. To avoid the high computational demands of approaches such as Computational Fluid Dynamics (CFD) [5]-[9], which are unsuitable for system stability analysis and on-board control design, [7], [10], simplified slosh models that reasonably describe sloshing effects are often used for control design purposes [10]-[13], [17]-[20]. Of these, the adopted here mass-spring-damper (MSD) is most suitable [6].

Among the various models for flexible bodies, the Euler-Bernoulli beam theory is adopted here. The approach developed herein can be adapted for different models if kinematics and kinetics separability in time and space holds.

Very few works have focused on SMS System Identification (SYSID), considering also fuel sloshing and flexible appendages. In [14], the SMS manipulator parameters are assumed known, while the flexible appendage is modeled as a lumped system; the sloshing effect is modeled as a pendulum, which is adequate during the orbital boost phase [16]. An MSD sloshing model parameter identification in zero-gravity using available measurements, was reported [6]. However, no methodologies exist to identify the SMS inertial parameters in the presence of both sloshing fuel and flexible appendages, while also identifying their parameters, including the authors' preliminary past work, e.g., [2], [6]; previously, S/Cs only with fuel sloshing [6], [13] or only with an appendage [8], have been studied, or the manipulator parameters were assumed to be known [14].

The performance of advanced model-based controllers can be improved by SYSID by providing more accurate models. Also, SYSID is useful in control design, both by not exciting system natural frequencies, and by allowing the design of robust controllers to compensate for parametric uncertainty.

This work focuses on the identification of a system including a S/C, its manipulator(s), sloshing effects modeled as a 3D MSD, and a flexible appendage modeled as a Euler-Bernoulli beam, see Figure 1. A novel SYSID scheme is developed, which identifies all parameters required for the reconstruction of the full system dynamics despite the unmeasurable sloshing and modal states. This is resolved using two experiments. In Experiment 1, all sloshing model parameters and the SMS base mass are identified, while modal analysis identifies the required modal parameters. In Experiment 2, all SMS inertial parameters are identified. The parameters obtained can predict system behavior fully and the developed scheme is validated by simulation. A Model-based PD controller combined with H_∞, provides a robust controller, similar to the one in [19], but for a spatial system. For the first time, the performance of this controller is shown to be significantly enhanced because of the SYSID output.

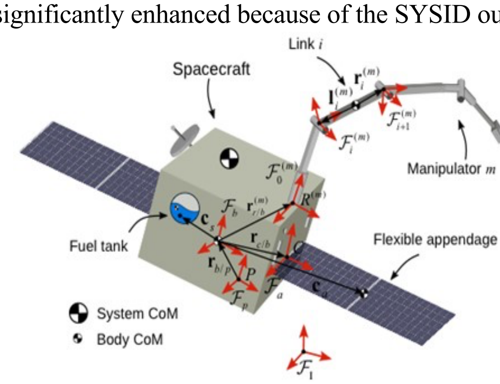

Figure 1. SMS with a 3D sloshing model and flexible solar panels.

II. SYSTEM DYNAMICS

The dynamics of the system under study are outlined here. The *system* consists of a S/C equipped with N_{rw} reaction wheels (RWs), n rigid manipulators with the m^{th} manipulator

*This work was supported partly by the European Space Agency (ESA), through the project *Guidance, navigation, and control of In-Orbit Assembly of large aNTennas* (IOANT).
[1] School of Mechanical Engineering, National Technical Univ. of Athens, 15780 Athens, Greece, (e-mail: {georek, egpapado}@central.ntua.gr).

consisting of N_m links, a flexible appendage $\mathcal{A}$, and a fuel tank exhibiting sloshing, Figure 1. To study the sloshing effect, a 3D mechanical equivalent MSD sloshing model is employed, [6]. To derive the dynamics compactly, the *base* consists of the S/C, the *stationary* fuel mass part and the RWs, with the *sloshing* fuel mass part and the flexible appendage excluded, and the *space manipulator system* is defined as consisting of the *base* and all manipulators.

A body frame $\mathcal{F}_b$ $\{X_b, Y_b, Z_b\}$ is attached at the *base* Center of Mass (CM). A *feature point* P on the S/C is tracked, and an observation frame $\mathcal{F}_p$ $\{X_p, Y_p, Z_p\}$ also is attached to it, with same orientation to that of $\mathcal{F}_b$. A frame $\mathcal{F}_i^{(m)}\{X_i^{(m)}, Y_i^{(m)}, Z_i^{(m)}\}$ is attached to the SMS i^{th} link of the m^{th} manipulator using the modified Denavit-Hartenberg convention, and a reference frame for the m^{th} manipulator $\mathcal{F}_0^{(m)}\{X_0^{(m)}, Y_0^{(m)}, Z_0^{(m)}\}$ is considered. Frame $\mathcal{F}_\mathrm{I}$ $\{X_\mathrm{I}, Y_\mathrm{I}, Z_\mathrm{I}\}$ is a local frame with orbital speed. For short experiment times and neglecting microgravity and orbital mechanics effects as small compared to the control forces, $\mathcal{F}_\mathrm{I}$ is an inertial frame. A *connection point* C between the base and the flexible appendage is considered and body frame $\mathcal{F}_a$ $\{X_a, Y_a, Z_a\}$ is attached to point C, rigidly fixed to the undeformed appendage. The $\bar{\bullet}$ denotes a column vector in frame $\mathcal{F}_\mathrm{I}$. A missing overbar indicates a column vector in frame $\mathcal{F}_b$.

The sloshing fuel oscillation is represented by a 3D MSD mechanical equivalent, with spring $k_{s,x}$, $k_{s,y}$, $k_{s,z}$ and damper constants $b_{s,x}$, $b_{s,y}$, $b_{s,z}$ along the $\mathcal{F}_b$ axes. The sloshing mass position $\mathbf{r}_s$ and velocity $\mathbf{v}_s$,with respect to the $\mathcal{F}_\mathrm{I}$ origin are

$$\mathbf{r}_s = \mathbf{r}_b + \mathbf{c}_s + \boldsymbol{\rho}_s \tag{1}$$

$$\mathbf{v}_s = \mathbf{v}_b + \dot{\boldsymbol{\rho}}_s + \boldsymbol{\omega}_b^\times(\mathbf{c}_s + \boldsymbol{\rho}_s) \tag{2}$$

where $\mathbf{r}_b$ gives the base CM position, $\mathbf{c}_s$ is the sloshing mass equilibrium position with respect to the base CM, $\boldsymbol{\rho}_s$ is the displacement of the sloshing mass from its equilibrium point, $\mathbf{v}_b$ is the base CM inertial linear velocity and $\boldsymbol{\omega}_b$ is the angular velocity of $\mathcal{F}_b$, all expressed in $\mathcal{F}_b$; and $\bullet^\times$ indicates a skew-symmetric matrix obtained from column vector $\bullet$.

The CM position of the i^{th} link of the m^{th} manipulator with respect to the origin of $\mathcal{F}_\mathrm{I}$, $\mathbf{r}_i^{(m)}$ is given by

$$\mathbf{r}_i^{(m)} = \mathbf{r}_b + \mathbf{r}_{r/b}^{(m)} + \sum_{k=1}^{i-1}\left(\mathbf{r}_k^{(m)} - \mathbf{l}_k^{(m)}\right) - \mathbf{l}_i^{(m)} \tag{3}$$

where $\mathbf{r}_{r/b}^{(m)}$ is a body-fixed vector for the position of point $\mathrm{R}^{(m)}$ with respect to the base CM, and $\mathbf{l}_i^{(m)}$, $\mathbf{r}_i^{(m)}$ are body-fixed vectors locating frames $\mathcal{F}_i^{(m)}$ and $\mathcal{F}_{i+1}^{(m)}$, from the i^{th} link CM, see Figure 1. The linear velocity of the i^{th} link CM of the m^{th} manipulator with respect to the $\mathcal{F}_\mathrm{I}$ origin is

$$\mathbf{v}_i^{(m)} = \mathbf{v}_b + \boldsymbol{\omega}_b^\times \mathbf{r}_{r/b}^{(m)} + \sum_{k=1}^{i-1}\boldsymbol{\omega}_k^{(m)\times}\left(\mathbf{r}_k^{(m)} - \mathbf{l}_k^{(m)}\right) - \boldsymbol{\omega}_i^{(m)\times}\mathbf{l}_i^{(m)} \tag{4}$$

where $\boldsymbol{\omega}_i^{(m)}$ is the i^{th} link/m^{th} manipulator angular velocity.

It can be shown that the inertial CM position of the deformed appendage $\mathbf{r}_a$ is

$$\mathbf{r}_a = \mathbf{r}_b + \mathbf{c}_a + \mathbf{L}_{t,c}^{\mathrm{T}}\boldsymbol{\delta} / m_a \tag{5}$$

where $\mathbf{c}_a$ is the CM position of the undeformed appendage with respect to base CM, m_a is the appendage mass, $\mathbf{L}_{t,c}$ is the translational modal participation matrix calculated at C, and $\boldsymbol{\delta}$ is the vector of modal coordinates consisting of the time amplitudes associated to the appendage mode shapes.

A. System CM and Momentum Equations

The position of the system CM, $\mathbf{r}_{cm}$, is related to $\mathbf{r}_s$ and $\mathbf{r}_a$ as

$$m_b\mathbf{r}_b + \sum_{m=1}^{n}\sum_{i=1}^{N_m} m_i^{(m)}\mathbf{r}_i^{(m)} + m_s\mathbf{r}_s + m_a\mathbf{r}_a = M\mathbf{r}_{cm} = M\mathbf{R}_b^{\mathrm{T}}\bar{\mathbf{r}}_{cm} \tag{6}$$

where m_b is the mass of the base, $m_i^{(m)}$ is the mass of the SMS i^{th} link of the m^{th} manipulator, m_s is the sloshing point mass, and M is the total mass, i.e., $M = m_b+m_r+m_s+m_a$, where m_r is the manipulator(s) total mass. The rotation matrix $\mathbf{R}_b$ describes frame $\mathcal{F}_b$ orientation with respect to frame $\mathcal{F}_\mathrm{I}$.

The system linear momentum $\mathbf{p}$ is the sum of the linear momenta of the base $\mathbf{p}_b$, all SMS links, sloshing mass $\mathbf{p}_s$ and flexible appendage $\mathbf{p}_a$

$$\begin{aligned}\mathbf{p} = \mathbf{p}_b + \sum_{m=1}^{n}\sum_{i=1}^{N_m}\mathbf{p}_i^{(m)} + \mathbf{p}_s + \mathbf{p}_a = m_b\mathbf{v}_b + \sum_{m=1}^{n}\sum_{i=1}^{N_m} m_i^{(m)}\mathbf{v}_i^{(m)} + \\ + m_s\mathbf{v}_s + m_a\mathbf{v}_b + \boldsymbol{\omega}_b^\times\left(m_a\mathbf{c}_a + \mathbf{L}_{t,c}^{\mathrm{T}}\boldsymbol{\delta}\right) + \mathbf{L}_{t,c}^{\mathrm{T}}\dot{\boldsymbol{\delta}} = M\mathbf{v}_{cm}\end{aligned} \tag{7}$$

where $\mathbf{p}_i^{(m)}$ is the linear momentum of the SMS i^{th} link of the m^{th} manipulator, $\mathbf{v}_{cm}$ is the velocity of the system CM. The system angular momentum $\mathbf{h}$ with respect to the $\mathcal{F}_\mathrm{I}$ origin, is the sum of the angular momenta of the base $\mathbf{h}_b$, all SMS links, the sloshing mass $\mathbf{h}_s$, and the flexible appendage $\mathbf{h}_a$

$$\mathbf{h} = \mathbf{h}_b + \sum_{m=1}^{n}\sum_{i=1}^{N_m}\mathbf{h}_i^{(m)} + \mathbf{h}_s + \mathbf{h}_a = \mathbf{h}_b + \sum_{m=1}^{n}\sum_{i=1}^{N_m}\mathbf{h}_i^{(m)} + m_s\mathbf{r}_s^\times\mathbf{v}_s + \mathbf{h}_a \tag{8}$$

where the base angular momentum $\mathbf{h}_b$ and the SMS i^{th} link of the m^{th} manipulator angular momentum $\mathbf{h}_i^{(m)}$ are as in [6]. Also, the $\mathbf{h}_a$ is given by

$$\begin{aligned}\mathbf{h}_a = \mathbf{I}_{a,b}\boldsymbol{\omega}_b + \left(\mathbf{L}_{r,c}^{\mathrm{T}} + \mathbf{r}_{c/b}^\times\mathbf{L}_{t,c}^{\mathrm{T}}\right)\dot{\boldsymbol{\delta}} + \left(m_a\mathbf{c}_a + \mathbf{L}_{t,b}^{\mathrm{T}}\boldsymbol{\delta}\right)^\times\mathbf{v}_b + \\ + \mathbf{r}_b^\times\left(m_a\mathbf{v}_b + \boldsymbol{\omega}_b^\times\left(m_a\mathbf{c}_a + \mathbf{L}_{t,c}^{\mathrm{T}}\boldsymbol{\delta}\right) + \mathbf{L}_{t,c}^{\mathrm{T}}\dot{\boldsymbol{\delta}}\right)\end{aligned} \tag{9}$$

where $\mathbf{L}_{r,c}$ is the rotational modal participation matrix calculated at point C.

B. System Equations of Motion

The system equations of motion are derived using a Lagrangian approach, with T the system kinetic energy, V its potential energy and $\mathfrak{I}$ a dissipation function [23]

$$\frac{d}{dt}\left(\frac{\partial T}{\partial \mathbf{v}_b}\right) + \boldsymbol{\omega}_b^\times\frac{\partial T}{\partial \mathbf{v}_b} = \mathbf{f}_e \tag{10}$$

$$\frac{d}{dt}\left(\frac{\partial T}{\partial \boldsymbol{\omega}_b}\right) + \boldsymbol{\omega}_b^\times\frac{\partial T}{\partial \boldsymbol{\omega}_b} + \mathbf{v}_b^\times\frac{\partial T}{\partial \mathbf{v}_b} = \mathbf{n}_e \tag{11}$$

$$\frac{d}{dt}\left(\frac{\partial T}{\partial \dot{\boldsymbol{\rho}}_s}\right) + \boldsymbol{\omega}_b^\times\frac{\partial T}{\partial \dot{\boldsymbol{\rho}}_s} = -\frac{\partial \mathfrak{I}}{\partial \dot{\boldsymbol{\rho}}_s} - \frac{\partial V}{\partial \boldsymbol{\rho}_s} = -\left(\mathbf{K}_s\boldsymbol{\rho}_s + \mathbf{B}_s\dot{\boldsymbol{\rho}}_s\right) \tag{12}$$

$$\frac{d}{dt}\left(\frac{\partial T}{\partial \dot{\boldsymbol{\delta}}}\right) + \boldsymbol{\omega}_b^\times\frac{\partial T}{\partial \dot{\boldsymbol{\delta}}} = -\frac{\partial \mathfrak{I}}{\partial \dot{\boldsymbol{\delta}}} - \frac{\partial V}{\partial \boldsymbol{\delta}} = -\left(\mathbf{K}_a\boldsymbol{\delta} + \mathbf{B}_a\dot{\boldsymbol{\delta}}\right) \tag{13}$$

$$\frac{d}{dt}\left(\frac{\partial T}{\partial \dot{\mathbf{q}}_{rw}}\right) = \boldsymbol{\tau}_{rw} \qquad i = 1, \ldots, N_{rw} \tag{14}$$

$$\frac{d}{dt}\left(\frac{\partial T}{\partial \dot{\mathbf{q}}_r}\right) - \frac{\partial T}{\partial \mathbf{q}_r} = \boldsymbol{\tau}_r \tag{15}$$

where $\mathbf{f}_e$ is the resulting external force applied on the S/C by its thrusters and $\mathbf{n}_e$ is the associated moment. $\mathbf{K}_s, \mathbf{K}_a$, and $\mathbf{B}_s, \mathbf{B}_a$ are spring and damping matrices for sloshing and the appendage, $\mathbf{q}_r$, $\dot{\mathbf{q}}_r$ are the SMS joint angles and rates, respectively, and $\boldsymbol{\tau}_r$, $\boldsymbol{\tau}_{rw}$ are the torques applied on the manipulator joints and RWs, respectively.

III. System Identification Method

The main challenge for the parameter identification of an SMS with sloshing and flexible appendage(s) stems from the fact that sloshing, and modal (flexible) states are both unmeasurable, e.g., the velocity or acceleration of m_s cannot be measured. To perform parametric SYSID using a regressor formulation (**Y**$\boldsymbol{\pi}$**=b; Y:** regressor, $\boldsymbol{\pi}$**:** parameter vector, **b:** inputs), the selected equations must be expressed linearly with respect to the unknowns. For the system under study, if its equations are written in such form, the coefficients of the unknown parameters are functions not only of the measurable quantities, such as S/C states but also of unmeasurable quantities, such as sloshing and modal states. This is tackled next by employing two experiments.

A. System identification Exp. 1

In *Exp. 1*, the S/C orientation is kept constant; only net forces are applied to it, resulting in pure translation. Modal analysis is performed to identify the modal parameters of the flexible appendage(s), using *Covariance based Stochastic Subspace Identification* (SSI-COV). The measurements used are the accelerations of flexible appendage's tracked points i.e., those whose motion is measured by a sensor mounted on them. Moreover, the pure translational motion allows one to *eliminate the unmeasurable sloshing and modal states* from the equation that yields the *regressor*, while also *decoupling the sloshing identification from the modal parameter identification*, lowering the complexity of the process, and avoiding possible error propagation issues; then, only measurable S/C and joint states are required. During this experiment, the manipulator(s) joints are locked, and thus the SMS behaves as a rigid body. With this experiment, all sloshing parameters and the SMS base mass are identified.

Using (10) and (12) with zero $\boldsymbol{\omega}_b$, $\dot{\boldsymbol{\omega}}_b$, and setting the base inertial linear acceleration $\dot{\mathbf{v}}_b$ as $\mathbf{a}_b$, the required system equations of motion for translation are

$$m_r\mathbf{a}_b - \mathbf{K}_s\boldsymbol{\rho}_s - \mathbf{B}_s\dot{\boldsymbol{\rho}}_s = \mathbf{f}_e - \mathbf{L}_{t,c}^{\mathrm{T}}\ddot{\boldsymbol{\delta}} = \mathbf{f}^* \tag{16}$$

$$m_s\mathbf{a}_s + \mathbf{K}_s\boldsymbol{\rho}_s + \mathbf{B}_s\dot{\boldsymbol{\rho}}_s = \mathbf{0} \tag{17}$$

where mass $m_r = M - m_s$, and $\mathbf{a}_s$ is the inertial linear acceleration of the sloshing point mass

$$\mathbf{a}_s = \mathbf{a}_b + \ddot{\boldsymbol{\rho}}_s \tag{18}$$

Equations (16) and (17) include the unmeasurable sloshing and modal states, which must be eliminated. For ease, this is done via a Laplace transformation. Considering the scalar form of (16) and (17) for axis *i*, ($i = x, y, z$), and sloshing fuel initially at rest, use of the Laplace transform yields

$$m_r\, s v_{b,i} - k_{s,i}(r_{s,i} - r_{b,i} - c_{s,i}) - b_{s,i}(s\, r_{s,i} - v_{b,i}) = f_i^* \tag{19}$$

$$m_s s^2 r_{s,i} + k_{s,i}(r_{s,i} - r_{b,i} - c_{s,i}) + b_{s,i}(s\, r_{s,i} - v_{b,i}) = 0 \tag{20}$$

where all variables are in the Laplace domain. Solving (20) for $r_{s,i}(s)$, substituting in (19), and considering the base CM velocity as the output, the transfer function $G_s(s)$ for axis *i* is

$$G_i(s) = \frac{v_{b,i}(s)}{f_i^*(s)} = \frac{s^2 + b_{s,i}/m_s s + k_{s,i}/m_s}{m_r s\left(s^2 + b_{s,i}(M/m_b\, m_s)s + k_{s,i}(M/m_b\, m_s)\right)} \tag{21}$$

Then, inverse Laplace is employed to relate $v_{b,i}$ to f_i^* in a differential equation. The base inertial linear acceleration $a_{b,i}$ is a measurable state; double integration is performed to avoid noisy differentiations:

$$\begin{aligned} -\frac{1}{m_r} f_i^* - \frac{k_{s,i}}{m_r m_s}\int_0^t\!\!\int_0^t f_i^* dt dt + k_{s,i}\frac{M}{m_r\, m_s}\int_0^t\!\!\int_0^t a_{b,i} dt dt - \\ -\frac{b_{s,i}}{m_r m_s}\int_0^t f_i^* dt + b_{s,i}\frac{M}{m_r\, m_s}\int_0^t a_{b,i} dt = -a_{b,i} \end{aligned} \tag{22}$$

Since the rigid system just translates in Exp. 1 and assuming no traction or y-bending in the flexible appendage, i.e.,

$$\mathbf{L}_{t,j}^{\mathrm{T}}\ddot{\boldsymbol{\delta}}(t) = \mathbf{L}_{t,j}^{\mathrm{T}}\dot{\boldsymbol{\delta}}(t) = \mathbf{L}_{t,j}^{\mathrm{T}}\boldsymbol{\delta}(t) = 0, \quad \text{for } j = x, y \tag{23}$$

it can be shown that (22), yields equations for $i = x, y$ that can be written linearly with respect to the parameters $\boldsymbol{\pi} = \boldsymbol{\pi}_{G,i}$

$$\boldsymbol{\pi}_{G,i} = \left[\frac{1}{m_r}, \frac{k_{s,i}}{m_r\, m_s}, k_{s,i}\frac{M}{a_1 m_s}, \frac{b_{s,i}}{a_1\, m_s}, b_{s,i}\frac{M}{a_1 m_s}\right]^{\mathrm{T}} \tag{24}$$

With regressor $\mathbf{Y}$=$\mathbf{Y}_{G,i}(t)$ and inputs $b = b_{G,i}(t)$ as

$$\mathbf{Y}_{G,i} = \left[-f_{e,i}, -\iint_0^t f_{e,i} dt dt\ , \iint_0^t a_{b,i} dt dt, -\int_0^t f_{e,i} dt, \int_0^t a_{b,i} dt\right] \tag{25}$$

$$b_{G,i} = -a_{b,i}(t) \tag{26}$$

where $\mathbf{Y}_{G,i}$ are of full rank by design, and are obtained numerically using ode45 in Matlab/Simulink. For i = z, and in the presence of *z*-bending, the same procedure results in

$$\boldsymbol{\pi}_{G,z} = \frac{1}{m_r}\left[1,\ \rho,\ \frac{k_{s,z}}{m_s},\ \frac{k_{s,z}\rho}{m_s},\ \frac{k_{s,z}M}{m_s},\ \frac{b_{s,z}}{m_s},\ \frac{b_{s,z}\rho}{m_s},\ \frac{b_{s,z}M}{m_s}\right]^{\mathrm{T}} \tag{27}$$

where ρ is the appendage linear average density, while $\mathbf{Y}_{G,z}$ is a function of $a_{b,z}$, $f_{e,z}$ and the acceleration, velocity, position of flexible appendage(s) tracked points, and $b_{G,z}$ is as in (26).

Taking *N* measurements of accelerations $a_{b,i}$ and of the appendage accelerometers, and computing numerically their first and double integrals at times $t_1, t_2, \ldots, t_N$, an overdetermined system of equations is obtained for each axis *i* which can be solved to yield $\boldsymbol{\pi}_{G,i}$. For $i = x, y$, the 4 unknown parameters M, m_s, $k_{s,i}$, $b_{s,i}$ are found, while for $i = z$ the same parameters as well as ρ and m_r are identified.

All required measurements are provided by an IMU sensor mounted at some point P on the S/C, with the IMU providing the linear acceleration $\mathbf{a}_p$ of point P, equal to that of the base $\mathbf{a}_b$, and by accelerometers on flexible appendage tracked points. The first and double integrals of the accelerations are calculated with zero initial conditions, and with the origin of $\mathcal{F}_I$ taken at the initial location of point P.

B. System identification Exp. 2

In *Exp. 2*, the system is in the free-floating mode with zero initial momentum, i.e., no external forces/ moments act on it; only RWs and manipulator(s) motors are active, applying internal torques. In these conditions, the system CM remains fixed in $\mathcal{F}_I$, [24]. Exp. 2 and associated method are designed to bypass the need for unmeasurable sloshing states, and an estimator is developed for the unmeasurable modal states.

Identification equation

The system is in free-floating mode and its inertial angular momentum $\bar{\mathbf{h}}$ is conserved to its initial value $\mathbf{h}_{in}$,

$$\bar{\mathbf{h}} = \mathbf{R}_b \mathbf{h} \overset{(8)}{=} \mathbf{R}_b (\mathbf{h}_b + \sum_{m=1}^{n}\sum_{i=1}^{N_m} \mathbf{h}_i^{(m)} + m_s \mathbf{r}_s^{\times} \mathbf{v}_s + \mathbf{h}_a) = (\mathbf{R}_b)_{in} \mathbf{h}_{in} \quad (28)$$

Elimination of sloshing states

Note that (28) cannot be directly used for identification since the sloshing mass inertial position $\mathbf{r}_s$ and velocity $\mathbf{v}_s$ are functions of the unmeasurable sloshing states $\boldsymbol{\rho}_s$, $\dot{\boldsymbol{\rho}}_s$.

To tackle this shortcoming, the conservation of system linear momentum and the system CM equations are employed. Specifically, the system linear momentum $\bar{\mathbf{p}}$ projected in frame $\mathcal{F}_{I}$, is conserved in the free-floating mode, and assuming zero system initial linear momentum, it yields

$$\mathbf{v}_s = -(\mathbf{p}_b + \sum_{m=1}^{n}\sum_{i=1}^{N_m} \mathbf{p}_i^{(m)} + \mathbf{p}_a)/m_s \quad (29)$$

Solving (6) for $m_s\mathbf{r}_s$ and substituting it in (8), along with $\mathbf{v}_s$ from (29), $\mathbf{h}_a$ from (9), and $\mathbf{h}_b$, $\mathbf{h}_i^{(m)}$ as given in [6], a model set results, which contains only the S/C and the modal states, while the sloshing states are no longer required. Note that, since $\bar{\mathbf{v}}_{cm}$ is zero, $\bar{\mathbf{r}}_{cm}$ is a constant vector, which can be treated as a constant unknown parameter to be estimated.

Moreover, the base CM inertial position $\mathbf{r}_b$ and velocity $\mathbf{v}_b$ in $\mathbf{h}_b$ (see [6]) can be substituted by kinematic equations:

$$\mathbf{r}_b = \mathbf{r}_p - \mathbf{r}_{p/b} \quad \mathbf{v}_b = \mathbf{v}_p - \boldsymbol{\omega}_b^{\times} \mathbf{r}_{p/b} \quad (30)$$

where $\mathbf{r}_p$, $\mathbf{v}_p$, are the inertial position and linear velocity respectively, of the tracked point P on the S/C i.e., where the IMU sensor is mounted, and $\mathbf{r}_{p/b}$ is the position vector of point P, with respect to the base CM. Vector $\mathbf{r}_{p/b}$ is considered as unknown parameter to be estimated by the identification scheme; once estimated, it renders the base CM known.

Modal states estimator

To implement the developed approach which eliminates unmeasurable sloshing states, the unmeasurable modal states $\mathbf{z} = [\mathbf{z}_1^{\mathrm{T}} \quad \mathbf{z}_2^{\mathrm{T}}]^{\mathrm{T}} = [\boldsymbol{\delta}^{\mathrm{T}} \quad \dot{\boldsymbol{\delta}}^{\mathrm{T}}]^{\mathrm{T}}$ must be estimated. It can be shown that, by taking N_a measurements from N_a accelerometers on the flexible panel, then

$$\dot{\mathbf{z}} = \begin{bmatrix} \dot{\boldsymbol{\delta}} \\ \ddot{\boldsymbol{\delta}} \end{bmatrix} = \begin{bmatrix} \dot{\mathbf{z}}_1 \\ \dot{\mathbf{z}}_2 \end{bmatrix} = \begin{bmatrix} \mathbf{z}_2 \\ \boldsymbol{\Phi}^{*-1}\left(-\mathbf{A} - \mathbf{B}(\mathbf{z}_1) - \mathbf{C}(\mathbf{z}_2)\right) \end{bmatrix} \quad (31)$$

where $\boldsymbol{\Phi}^*$ is a function of the mode shapes, identified from Exp. 1, while matrices $\mathbf{A}$, $\mathbf{B}$ and $\mathbf{C}$ are functions of the identified modal shapes, and the SMS base linear and angular acceleration and angular velocity, and of the panel accelerometer measurements, all of which are available. Then, the modal states $\mathbf{z}$ can be estimated at time step k by

$$\mathbf{z}(k) = \mathbf{z}(k-1) + \dot{\mathbf{z}}(k)T_s \quad (32)$$

where T_s is the sampling time.

Two steps of regressor formulation

A two-step scheme is devised i.e., Step A and Step B, and thus two distinct regressor formulations result. In Step A, the constant location of the system CM $\bar{\mathbf{r}}_{cm}$ is estimated. In Step B, the SMS inertial parameters are estimated, knowing M, m_s, and $\bar{\mathbf{r}}_{cm}$ from Exp. 1 and Step A of Exp. 2, respectively.

In *Step A*, the linear velocity $\mathbf{v}_p$ is written as a function of the CM inertial position $\bar{\mathbf{r}}_{cm}$, estimated based on the position and velocity barycentric analysis in [21], extended here to include the sloshing and modal effect

$$\mathbf{v}_p = \mathbf{R}_b^{\mathrm{T}}\bar{\mathbf{v}}_{cm} + \boldsymbol{\omega}_b^{\times}\left(\mathbf{r}_p - \mathbf{R}_b^{\mathrm{T}}\bar{\mathbf{r}}_{cm}\right) + \sum_{m=1}^{n}\sum_{k=1}^{N_m}\left[\dot{q}_{r,i}^{(m)}\mathbf{z}_i^{(m)}\right]^{\times}\tilde{\mathbf{l}}_i^{(m)} - \\ - m_s\dot{\boldsymbol{\rho}}_s / M - \mathbf{L}_{t,c}^{\mathrm{T}}\dot{\boldsymbol{\delta}} / M \quad (33)$$

where $\mathbf{z}_i^{(m)}$ is the unit vector along the axis of rotation of the i^{th} joint of the m^{th} manipulator. Eq. (33) can be written linearly with respect to the unknown parameters,

$$\mathbf{R}_b^{\mathrm{T}}\bar{\mathbf{v}}_{cm} - \boldsymbol{\omega}_b^{\times}\mathbf{R}_b^{\mathrm{T}}\bar{\mathbf{r}}_{cm} + \mathbf{Y}_{r,cm}(\mathbf{q}_r, \dot{\mathbf{q}}_r)\boldsymbol{\pi}_{r,cm} = \mathbf{v}_p - \boldsymbol{\omega}_b^{\times}\mathbf{r}_p + \mathbf{L}_{t,c}^{\mathrm{T}}\dot{\boldsymbol{\delta}}/M \quad (34)$$

where vector $\boldsymbol{\pi}_{r,cm}$ includes SMS inertial parameters. Note that in (34) the sloshing state $(m_s/M)\dot{\boldsymbol{\rho}}_s$ has been neglected since $\dot{\boldsymbol{\rho}}_s$ is in general small and the total mass M very large; this was also validated in a simulation study. The $\mathbf{Y}_{r,cm}$ also requires the mass M, estimated in Exp. 1, while the modal state rates $\dot{\boldsymbol{\delta}}$ are estimated by the presented estimator in (32).

Hence, the unknown parameters set a vector $\boldsymbol{\pi} = \boldsymbol{\pi}_{cm}$, with regressor $\mathbf{Y} = \mathbf{Y}_{cm}(t)$ and $\mathbf{b} = \mathbf{b}_{cm}(t)$ where

$$\mathbf{Y}_{cm}(t) = \left[\mathbf{R}_b^{\mathrm{T}}(t), \quad -\boldsymbol{\omega}_b^{\times}(t)\mathbf{R}_b^{\mathrm{T}}(t), \quad \mathbf{Y}_{r,cm}(\mathbf{q}_r(t), \dot{\mathbf{q}}_r(t))\right] \quad (35)$$

$$\mathbf{b}_{cm}(t) = \mathbf{v}_p(t) - \boldsymbol{\omega}_b^{\times}(t)\mathbf{r}_p(t) + \mathbf{L}_{t,c}^{\mathrm{T}}\dot{\boldsymbol{\delta}} / M \quad (36)$$

$$\boldsymbol{\pi}_{cm} = [\ \bar{\mathbf{v}}_{cm}^{\mathrm{T}} \quad \bar{\mathbf{r}}_{cm}^{\mathrm{T}} \quad \boldsymbol{\pi}_{r,cm}^{\mathrm{T}}\ ]^{\mathrm{T}} \quad (37)$$

Taking N measurements of the variables $\mathbf{r}_p$, $\mathbf{v}_p$, $\boldsymbol{\omega}_b$, (also used to obtain $\mathbf{R}_b$), and $\mathbf{q}_r$, $\dot{\mathbf{q}}_r$, at time instances t_1, t_2, …, t_N during Exp. 2, results in an overdetermined system of equations, which is solvable using the Total Least Squares (TLS) algorithm [25] to yield $\boldsymbol{\pi}_{cm}$ and, thus, $\bar{\mathbf{r}}_{cm}$.

In *Step B*, $\mathbf{h}$ and thus, also $\mathbf{h}_{in}$, in (28), are written linearly with respect to the SMS inertial parameters, grouped in a reduced vector $\boldsymbol{\pi} = \boldsymbol{\pi}_m$,

$$\mathbf{R}_b(t)\left[\mathbf{Y}_m(t)\boldsymbol{\pi}_{cm} - \mathbf{b}_m(t)\right] = (\mathbf{R}_b)_{in}\left[(\mathbf{Y}_m)_{in}\boldsymbol{\pi}_{cm} - (\mathbf{b}_m)_{in}\right] \quad (38)$$

which can be further written as

$$\left[\mathbf{R}_b(t)\mathbf{Y}_m(t) - (\mathbf{R}_b)_{in}(\mathbf{Y}_m)_{in}\right]\boldsymbol{\pi}_m = \mathbf{R}_b(t)\mathbf{b}_m(t) - (\mathbf{R}_b)_{in}(\mathbf{b}_m)_{in} \quad (39)$$

where the vector $\mathbf{b}_m$ requires knowledge of masses M, m_s and RWs moment of inertia $\mathbf{I}_{rw}$; M, m_s were estimated in Exp. 1, and $\mathbf{I}_{rw}$ was assumed to be known. Taking measurements of the variables $\mathbf{r}_p$, $\mathbf{v}_p$, $\boldsymbol{\omega}_b$, (again also used to obtain $\mathbf{R}_b$), and $\mathbf{q}_r$, $\dot{\mathbf{q}}_r, \dot{\mathbf{q}}_{rw}$, at N times t_1, t_2, …, t_N, yields an overdetermined system of equations, which is solved using the TLS algorithm yielding $\boldsymbol{\pi}_m$. In this scheme, propagating the identification relative errors of the parameters M, m_s and $\bar{\mathbf{r}}_{cm}$, identified already with very small relative errors from Exp. 1 and Exp. 2 – Step A, respectively (see Section V), does not distort the identified $\boldsymbol{\pi}_m$, while the other already identified parameters are not used in and do not affect the identification of $\boldsymbol{\pi}_m$.

Therefore, all SMS inertial parameters are identified while no unmeasurable sloshing/ modal states are needed. By employing the developed methodology and recursive TLS, previously known parameters can be used as an initial guess.

IV. Model-based PD Augmented by H∞ Control

The contribution of an accurate SYSID campaign on the control of an SMS, is demonstrated here using the identified inertial, sloshing, and modal parameters in a Model-based PD (MBPD) controller, without and with a robustness term developed by an H_∞ control scheme. A simultaneous control of both the manipulator and the SMS base attitude (thrusters assumed deactivated, e.g., for safety) is opted, while, without loss of generality, joint-space manipulator control is studied.

With negligible gravitational forces and other external disturbances, the reduced equations of motion of the 3D SMS in the joint space are derived from (10), (11), (14) and (15), without including the effects of fuel sloshing and flexible appendage directly in the model based part of the controller, but rather letting them act as disturbances. Thus, after some algebraic manipulations, the SMS joint-space reduced equations of motion, take the form

$$\mathbf{H}(\mathbf{q})\ddot{\mathbf{q}}+\mathbf{c}(\dot{\mathbf{q}},\mathbf{q})=\mathbf{J}_c^{\mathrm{T}}\mathbf{Q}_c \tag{40}$$

where $\mathbf{H}$ and $\mathbf{c}$ are the system inertia matrix and the nonlinear Coriolis/ centrifugal terms vector respectively, $\mathbf{J}_c$ is a Jacobian matrix, and

$$\mathbf{q}=\left[\mathbf{q}_b^{\mathrm{T}},\mathbf{q}_m^{\mathrm{T}}\right]^{\mathrm{T}} \tag{41}$$

$$\mathbf{Q}_c=\left[\boldsymbol{\tau}_{RW}^{\mathrm{T}},\boldsymbol{\tau}^{\mathrm{T}}\right]^{\mathrm{T}} \tag{42}$$

with $\mathbf{q}_b$, $\mathbf{q}_m$ being the vectors of the SMS base Euler Angles and the manipulator joint angles respectively, while $\mathbf{Q}_c$ is the control torques vector, i.e., RW torques $\boldsymbol{\tau}_{RW}$ (rendered to the base-frame axes) and manipulator joint torques $\boldsymbol{\tau}$.

Then, a MBPD controller takes the form

$$\mathbf{Q}_c=\hat{\mathbf{J}}_c^{-\mathrm{T}}\left(\hat{\mathbf{H}}\left(\ddot{\mathbf{q}}_d+\mathbf{K}_D\dot{\mathbf{e}}+\mathbf{K}_P\mathbf{e}\right)+\hat{\mathbf{c}}\right) \tag{43}$$

where $\mathbf{q}_d$ denotes the desired trajectory of $\mathbf{q}$, $\mathbf{e}=\mathbf{q}_d-\mathbf{q}$, and $\mathbf{K}_P$, $\mathbf{K}_D$ are control gain matrices. The term $(\hat{*})$ refers to an element obtained by use of the uncertain system parameters. Substituting $\mathbf{Q}_c$ from (43) into (40), yields

$$\ddot{\mathbf{e}}+\mathbf{K}_D\dot{\mathbf{e}}+\mathbf{K}_P\mathbf{e}=\mathbf{d}_u \tag{44}$$

where $\mathbf{d}_u$ is a function of the uncertainties and measurement noise and acts as a disturbance to the MBPD controller. Also, since (40) is not based on the complete system dynamics (fuel sloshing and flexible appendage(s) are not considered) as it is used to design the MBPD controller, substitution of $\mathbf{Q}_c$ in (43) in the complete system dynamics derived by the complete set of (10) to (15), will result in the system error dynamics as

$$\ddot{\mathbf{e}}+\mathbf{K}_D\dot{\mathbf{e}}+\mathbf{K}_P\mathbf{e}=\mathbf{d}_u+\mathbf{d}_d=\mathbf{d}_{tot} \tag{45}$$

where $\mathbf{d}_d$ is due to the fuel sloshing and the flexible appendage vibrations. If the disturbance term $\mathbf{d}_{tot}$ is relatively small, then it is quite possible that the MBPD controller of (43) will compensate for it, and perform as designed, with acceptable errors. Otherwise, an additional H_∞ control term can be added to (43), yielding

$$\mathbf{Q}_c=\hat{\mathbf{J}}_c^{-\mathrm{T}}\left(\hat{\mathbf{H}}\left(\ddot{\mathbf{q}}_d+\mathbf{K}_D\dot{\mathbf{e}}+\mathbf{K}_P\mathbf{e}\right)+\hat{\mathbf{c}}\right)+\mathbf{u}_\infty \tag{46}$$

adding further robustness to the controller (MBPD+H_∞). Then, the system error dynamics become

$$\ddot{\mathbf{e}}+\mathbf{K}_D\dot{\mathbf{e}}+\mathbf{K}_P\mathbf{e}=\mathbf{d}_{tot}+\mathbf{u}_\infty \tag{47}$$

The H_∞ term $\mathbf{u}_\infty$ can be a linear H_∞ controller, designed for the linearized left-hand side of (45) to compensate on the effect of $\mathbf{d}_{tot}$, similarly to the one presented in [19], but for a spatial system instead of a planar one.

V. Simulation Study

The developed method is applicable to multi-arm SMS; here it is illustrated by a spatial 3-DOF-arm, free-floating SMS. The kinematic and inertia parameters of the SMS are as in Table 1. The studied S/C is assumed to have 3 RWs in an orthogonal configuration, with $I_{rw,i}$=0.159 kgm^2. The position vector of the tracked point P on the base with respect to the base CM is $\mathbf{r}_{p/b}=[0.5,1.5,0.6]^{\mathrm{T}}$ m. The fuel CM (at rest) is at $\mathbf{c}_s=[0.03,-0.04,\ 0.05]^{\mathrm{T}}$ m, with respect to the base CM. The sloshing model parameters are shown in the *True Value* column of Table 2. The flexible appendage is modeled as a thin plate of size 6m x 3m x 0.003m, mounted at $\mathbf{r}_{c/b}$ = [1.5, 0, 0] with respect to the base CM.

Table 1. Parameters of the SMS in the Simulation Study.

i	l_i (m)	r_i (m)	m_i (kg)	I_{xx} (kg m^2)	I_{yy} (kg m^2)	I_{zz} (kg m^2)
0	-	$[-1,-1,1]^{\mathrm{T}}$	2000	1500	1500	1500
1	0.25	0.25	10	0.21	0.21	0.01
2	1.0	1.0	50	0.05	16.69	16.69
3	1.0	1.0	50	0.05	16.69	16.69

To obtain data for the SYSID, in Exp. 1 thrusters and RWs are employed, applying a net force and zero net moment. The applied force along S/C body frame axis i is given by

$$f_{e,i}=\begin{cases}40\ \mathrm{N} & t\le t_f/6\\ -40\ \mathrm{N} & t>t_f/6\ \text{and}\ t\le t_f/3\\ 0\ \mathrm{N} & t>t_f/3\end{cases} \tag{48}$$

where the duration t_f of Exp. 1 is 120 s.

In Exp. 2, only RWs and manipulator(s) are employed since the system operates in free-floating mode. The SMS is initially at rest. The system's angular momentum $\mathbf{h}_{in}$ is zero. The exciting torques applied by RWs, and manipulator motors are truncated Fourier series [26]. The Exp. 2 duration t_f is 80 s. The total duration for Exp. 1 and 2 is 200 s. In Matlab, the SYSID requires 7s, including signal processing; it will require much less with compiled code. IMU sensor and motor encoder realistic models, as in [6], are employed. IIR low-pass filters were used on the noisy measurements.

Simulation Results

Indicative simulated inputs and outputs for Exp. 1 and. 2 are shown in Figure 2. The SYSID results using noisy and filtered measurements for both Exp. 1 and 2 are displayed in Table 2 (using as ground truth a CFD-computed mass-spring-damper sloshing model and parameters) and Table 3, respectively. For brevity, only the four parameters with the two smallest and largest relative errors (%) are shown in Table 3. For Exp. 1, (24)-(26) were used, while for Exp. 2, (35)-(37) (Step A) and (39) (Step B) were employed. Only the relative errors of the estimated sloshing model damping coefficients $b_{s,i}$ are relatively large. However, the effect of these errors on S/C response prediction is negligible [6].

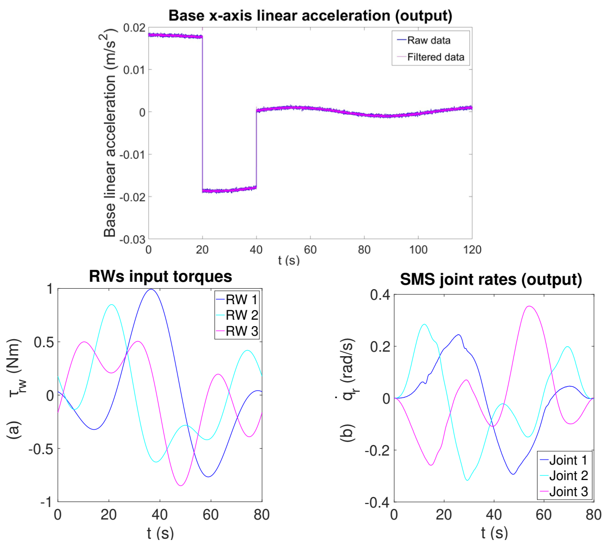

Figure 2. *Top*: Base x-axis linear acceleration for Exp. 1. *Bottom*: (a) RWs input torques, (b) SMS joint rates (output), for Exp. 2.

Overall, the system identification scheme developed computes all required parameters successfully, see Table 2 and Table 3. To demonstrate the importance of SYSID in the controlled system performance, simultaneous control of base attitude and manipulator in joint-space, is simulated, for the same SMS. Both MBPD (Eq. (43)) and MBPD+H$_\infty$ (Eq. (46)) controllers are tested, with nominal MBPD control gains as $\mathbf{K}_P = \mathbf{K}_D = diag(4,4,4)$. To demonstrate the importance of accurate knowledge of sloshing and flexible parameters, and specifically the natural frequencies of the corresponding elements, a different set of control gains is set, i.e., $\mathbf{K}_P = diag(.64,.64,.64)$, $\mathbf{K}_D = diag(1.6,1.6,1.6)$, that excite the third bending natural frequency of the flexible appendage. The H$_\infty$ part of MBPD+H$_\infty$ is designed for 5% parametric uncertainty levels, while simulations are run for various levels of parametric uncertainty in the controller model-based part.

TABLE 2. EXP. 1 TLS/ SSI-COV SYSID RESULTS (SI UNITS).

			True Value	Estimated Value	Rel. Error (%)
TLS	M		2256.8	2155.9	0.04
	m_s		49.6	49.9	0.6
	$k_{s,i}$		0.41	0.407	0.78
	$b_{s,i}$		0.02	-	>>
	ρ		2700	2761.17	2.266
SSI-COV	*Bending natural freq.*	1^{st}	0.046	0.0459	0.114
		2^{nd}	0.286	0.287	0.354
		3^{rd}	0.801	0.800	0.245

TABLE 3. EXP. 2 TLS SYSID RESULTS (MAX. AND MIN. ERRORS - SI UNITS).

	True Value	Estimated Value	Rel. Error (%)
$\pi_m(2)$	336028.408	335988.01	0.01
$\pi_m(7)$	3373.48	3374.04	0.02
$\pi_m(12)$	-1.06	-1.11	-4.80
$\pi_m(13)$	837.41	799.92	4.48

The desired trajectory for the SMS base attitude is to remain stationary. A desired trapezoidal profile for the three joint-angle velocities is used, with $a_0 = 0.001$ rad/s^2 for 20 s, then constant angular velocity for another 20 s, then a constant angular deceleration of $-a_0$ for another 20 s, and finally stationary desired angle for another 20 s. The same noise models in the measurements as before were used.

The maximum angle tracking errors $\mathbf{e}_b$ and $\mathbf{e}_i$ during the simulated control experiments in the presence of parametric uncertainties and measurement noise, are shown in Table 4. Case (C) with 5% uncertainty corresponds to the uncertainty levels for which the H$_\infty$ weighting matrices are designed.

As shown in Table 4, the more uncertain our estimation is regarding the system parameters, the larger the maximum relative error is, and even more so in case we accidentally excite one of the uncertain system natural frequencies. Moreover, it can be seen that a properly tuned H$_\infty$ augmentation of the MBPD, results in better performance, compared to the use of a bare MBPD. However, even in this case, a prior SYSID campaign resulting in parametric uncertainty within the tuned H$_\infty$ specifications and in knowledge of the system natural frequencies (so as not to exciting them), further increases the controller performance. Thus, 12.4% and 21.1% lower relative tracking errors for SMS base and joint angles respectively, are observed between cases (D) with SYSID use and (B) with 20% uncertainty, when using MBPD, while 5.2% and 15.2% are observed when using MBPD+H$_\infty$. The improvement rises to 87.9% and 86.7% when using MBPD and 14% and 22.2% when using MBPD+H$_\infty$, when comparing case (D) with SYSID use, to case (A) with 20% uncertainty and accidental excitation of one of the systems' natural frequencies.

TABLE 4. TRACKING ERRORS WITH VARIOUS LEVELS OF UNCERTAINTY

Gains	Uncertainty	Controller	$\mathbf{e}_b$	$\mathbf{e}_i$
$\mathbf{K}_{P,i} = \mathbf{K}_{D,i} = 4$ (no natural freq. excited)	**(D)** SYSID	MBPD	$1.70*10^{-4}$	$5.60*10^{-3}$
		MBPD+H$_\infty$	$2.75*10^{-5}$	$1.23*10^{-3}$
	(C) 5%	MBPD	$1.78*10^{-4}$	$5.87*10^{-3}$
		MBPD+H$_\infty$	$2.85*10^{-5}$	$1.28*10^{-3}$
	(B) 20% (No SYSID)	MBPD	$1.94*10^{-4}$	$7.10*10^{-3}$
		MBPD+H$_\infty$	$2.90*10^{-5}$	$1.45*10^{-3}$
$\mathbf{K}_{P,i} = 0.64$ $\mathbf{K}_{D,i} = 1.6$ (3rd bending freq. excited)	**(A) 20 %** (No SYSID)	MBPD	$1.41*10^{-3}$	$4.2*10^{-2}$
		MBPD+H$_\infty$	$3.2*10^{-5}$	$1.58*10^{-3}$

VI. CONCLUSION

This paper focused first on the identification of the parameters of a SMS including its sloshing and flexible appendage effects. Fuel sloshing was represented by a 3D MSD due to its suitability for control purposes. A novel system identification scheme, which identifies all system parameters in the presence of the unmeasurable sloshing and modal states, was developed. To bypass the need for the unmeasurable states, two identification experiments were designed. The significance of an accurate SYSID in the design and performance of a controller, was demonstrated by simulating a 3D SMS controlled by MBPD and MBPD+H$_\infty$ controllers, for enhanced robustness characteristics. In both cases, the use of the identified parameters and of control gains that do not excite the identified system natural frequencies, resulted in significant system performance improvements, while use of the uncertainty levels in the H$_\infty$ design further improved the system performance.

References

[1] Papadopoulos, E., Aghili, F., Ma, O., and Lampariello, R., “Robotic Manipulation and Capture in Space,” Frontiers: Robotics & AI - Space Robotics, 02 February 2022, doi: 10.3389/frobt.2022.849288.

[2] Christidi-Loumpasefski, O.O., Nguyen, D., Nanos, K., Rekleitis, G., Paraskevas, I., Regamey, Y.-J., Verhaeghe, A., Casu, D., Papadopoulos, E. and Ankersen, F., “Towards On-board Identification of Space Systems,” International Symposium on Artificial Intelligence, Robotics and Automation in Space, (i-SAIRAS ’20), October 19–23, 2020, Pasadena, California, USA.

[3] Ankersen, F., “Guidance, Navigation, Control and Relative Dynamics for Spacecraft Proximity Maneuvers,” *Ph.D. dissertation*, Dept. Electron. Syst., Aalborg Univ., Aalborg, Denmark, 2011.

[4] Slafer, L. I., and Challoner, A. D., “Propellant Interaction with the Payload Control System of Dual-Spin Spacecraft,” *Journal of Guidance, Control, and Dynamics,* Vol. 11, No. 4, 1988, pp. 343-351. doi.org/10.2514/3.20317.

[5] Feng, L., Baozeng, Y., Banerjee, A.K., Yong, T., Wenjun, W., and Zhengyong, L., “Large Motion Dynamics of In-Orbit Flexible Spacecraft with Large-Amplitude Propellant Slosh,” *Journal of Guidance, Control, and Dynamics*, Vol. 43, No. 3, March 2020. doi.org/10.2514/1.G004685.

[6] Christidi-Loumpasefski, O., Rekleitis, G., Papadopoulos, E., and Ankersen, F., “On System Identification of Space Manipulator Systems Including their Fuel Sloshing Effects,” *IEEE Robotics and Automation Letters (RA-L)*, Vol. 8, No. 5, pp. 2446-2453, May 2023.

[7] Baozeng, Y., Wenjun, W., and Yulong, Y., “Modeling and Coupling Dynamics of the Spacecraft with Multiple Propellant Tanks,” *AIAA Journal*, 2016. doi.org/10.2514/1.J055110.

[8] Li, W., Wang, D., Liu, C., "System Identification of Large Flexible Appendage on Satellite for Autonomous Control," *10th IEEE International Conference on Control and Automation* (ICCA), Hangzhou, China, June 12-14, 2013.

[9] Monti, R., *Physics of Fluids in Microgravity*, Taylor & Francis Publ., London, 2002, pp. 293-321. doi.org/10.1201/9781482265057.

[10] Allard, C.J., Ramos, M.D., and Schaub, H., “Spacecraft Dynamics Integrating Hinged Solar Panels and Lumped-Mass Fuel Slosh Model,” *AIAA/AAS Astrodynamics Specialist Conference*, 13 - 16 September 2016, Long Beach, CA. doi.org/10.2514/6.2016-5684.

[11] Dodge, F. T., “The New Dynamic Behavior of Liquids in Moving Containers,” *NASA Rept. SP-106*, Southwest Research Inst., San Antonio, TX, 2000.

[12] Reyhanoglu, M., and Hervas, J., “Nonlinear Control of a Spacecraft with Multiple Fuel Slosh Modes,” in *50th IEEE Conference on Decision and Control and European Control Conference (CDC-ECC),* 2011, pp. 6192–6197. doi.org/10.1109/CDC.2011.6160660.

[13] Reyhanoglu, M., and Hervas, J., “Nonlinear Control of Space Vehicles with Multi-Mass Fuel Slosh Dynamics,” in *5th International Conference on Recent Advances in Space Technologies (RAST)*, 2011, pp. 247–252. doi.org/10.1109/RAST.2011.5966834.

[14] Rackl, W., and Lampariello, R., “Parameter Identification of Free-Floating Robots with Flexible Appendages and Fuel Sloshing,” *Proc. International Conference on Modelling, Identification & Control*, Australia, December 3-5, 2014. doi.org/10.1109/icmic.2014.7020740.

[15] Ni, Z., Liu, J., Wu, Z., "Identification of the time-varying modal parameters of a spacecraft with flexible appendages using a recursive predictor-based subspace identification algorithm,” In Proc. of the Institution of Mechanical Engineers, Part G: Journal of Aerospace Engineering (Apr. 2018). doi: 10.1177/0954410018770560.

[16] Pirat, C., Ankersen, F., Walker, R., and Gass, V., “H_∞ and μ-Synthesis for Nanosatellites Rendezvous and Docking,” *IEEE Transactions on Control Systems Technology*, Vol. 28, No. 3, May 2020, pp. 1050 - 1057. doi.org/10.1109/TCST.2019.2892923.

[17] Fonseca, I. M. D., and Bainum, P. M., “CSI Due to Sloshing Motion on LEO LSS,” Advances in the Astronautical Sciences, Vol. 145, American Astronautical Society, Univelt, San Diego, CA, 2012, pp. 1073–1086.

[18] Lazzarin, M., Bettella, A., Manente, M., and Forno, R.D., “Analytical Sloshing Model and CFD Analysis for the Exomars Mission,” in *49th AIAA/ASME/SAE/ASEE Joint Propulsion Conference*, Jul 2013. doi.org/10.2514/6.2013-3842.

[19] Anastasiou, D., Nanos, K., and Papadopoulos, E., “Robust Model-based Hinf control for Free-floating Space Manipulator Cartesian Motions,” *30th IEEE Mediterranean Conference on Control and Automation*, (MED ‘22), Vouliagmeni, Greece, June 28-July 1, 2022.

[20] Utsumi, M., “Mechanical Models of Low-Gravity Sloshing Taking into Account Viscous Damping,” *Journal of Vibration and Acoustics*, Vol. 136, 2014. doi.org/10.1115/1.4025439.

[21] Moosavian, S. A. A., “Dynamics and Control of Free-Flying Manipulators Capturing Space Objects,” *PhD Thesis*, McGill University, Montreal, Canada, 1996.

[22] Goldstein, H., *Classical Mechanics*, Addison Wesley, 2nd ed., Reading, MA, 1980.

[23] Hughes, P. C., *Spacecraft Attitude Dynamics*, Series Dover Books on Engineering. Dover Publications, 2004.

[24] Papadopoulos, E., and Dubowsky, S., “On the Nature of Control Algorithms for Free-Floating Space Manipulators”, *IEEE Transactions on Robotics and Automation,* Vol. 7, No. 6, 1991, pp. 750-758. doi.org/10.1109/70.105384.

[25] Markovsky, I., and Van Huffel, S., “Overview of Total Least-Squares Methods,” *Signal Processing*, Vol. 87, No. 10, 2007, pp. 2283-2302. doi.org/10.1016/j.sigpro.2007.04.004.

[26] Christidi-Loumpasefski, O.-O., K. Nanos, and E. Papadopoulos, “On parameter estimation of space manipulator systems using the angular momentum conservation,” in *Proc. IEEE Int. Conf. Robot. Autom.*, Singapore, 2017, pp. 5453-5458.